S.1 Fabrication process for PDMS microfluidic channels with multilayered design
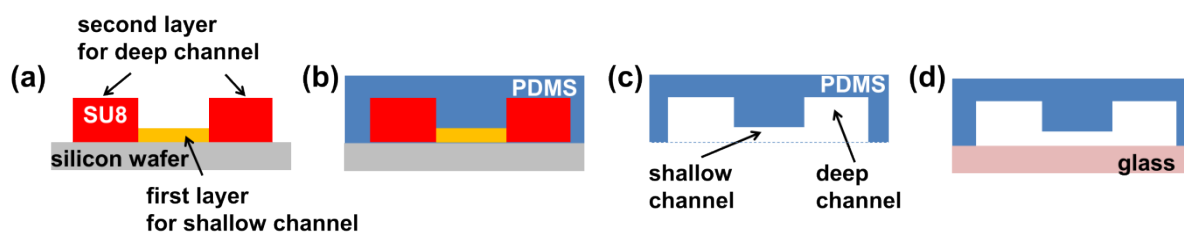

Figure S1 Scheme of the fabrication process for PDMS microfluidic channels with multilayered design.

Figure S1(a) - (d) shows schematic diagrams that describe the procedures for fabricating microfluidic devices with multilayered design. We fabricated microfluidic chips using the standard soft lithography: (a) A 4-inch silicon wafer was spin-coated with negative photoresist (SU-8 2025 or SU-8 2050, MicroChem Inc., target: 25 μm or 50 μm, this layer is only for the shallow channel), and then the coated silicon wafer was soft-baked for several minutes. The wafer was exposed under a mask using an aligner and placed on a hot-plate for several minutes of post-exposure baking, followed by a short relaxation time. Post-exposure baking was followed by development at room temperature, after which the whole wafer was rinsed with isopropyl alcohol (IPA) to clean the residues from the wafer. Subsequently, SU-8 2050 was patterned on the first SU-8 layer (target: 200 μm, this layer is for the deep channel) with same process as above. (b) A Polydimethylsiloxane (PDMS) precursor (Sylgard 184 Silicone Elastomer, Dow Corning) and a curing agent were mixed at a ratio of 10 to 1, based on weight. Before the PDMS mixture was poured onto the fabricated master, the master was silanized with (tridecafluoro-1,1,2,2,-tetrahydrooctyl)-1-trichlorosilane (Sigma Chemical Co., St. Louis, MO, USA) to allow easier removal of the PDMS after curing. The PDMS mixture was poured onto the master and cured at 95 °C for 1 h. (c) Then, the cured PDMS channel was peeled off from the master, cut and punched to connect microtubes. (d) The PDMS devices were directly bonded to a glass substrate without any surface treatment and then they were treated with oxygen plasma under 50 sccm of O$_2$ and 70 W for 40 s (Cute-MP, Femto Science, Korea).

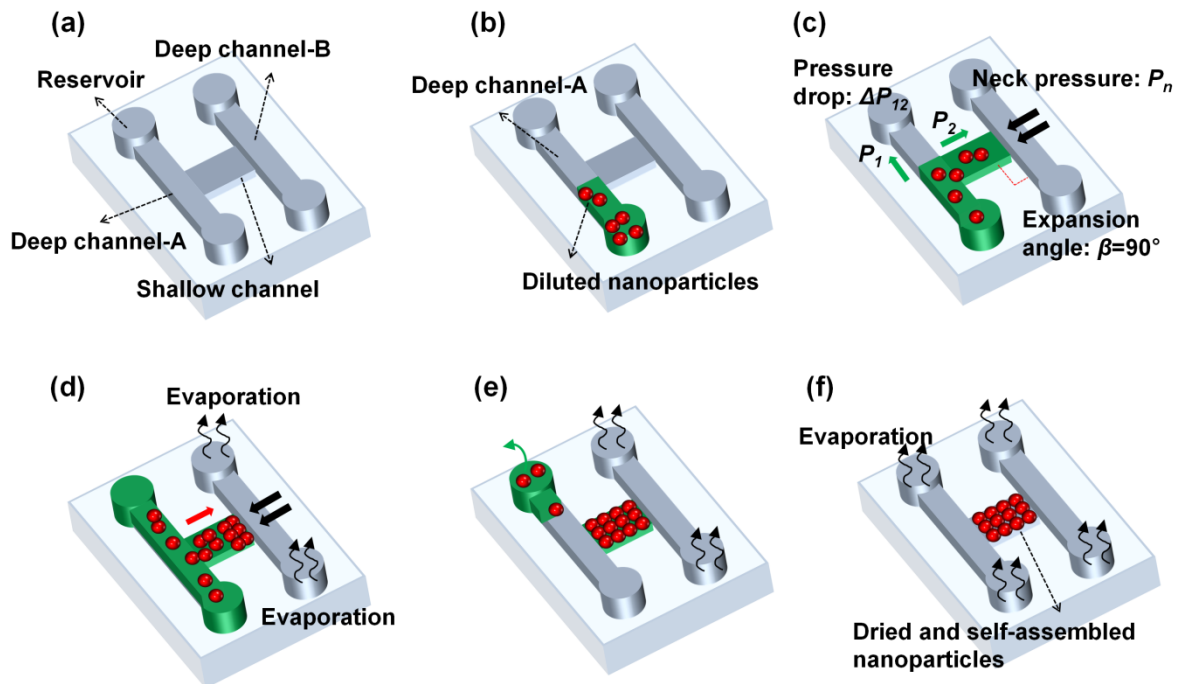## S.2 *In situ* formation of nanochannel networks membrane using nanoparticles

Figure S2 Fabrication process for the *in situ* formation of porous membranes using the self-assembly of particles within the PDMS channel

<Figure S2(a) and (b)>

(a) The PDMS device with shallow and deep channels was fabricated as described above. (b) In this paper, we used the diameter 100, 200, 300, and 700 nm of silica nanospheres and 100 nm of carboxylate polystyrene nanospheres. 100, 300, and 700 nm of silica nanospheres were purchased from Polyscience Inc., USA, and 200 nm of silica nanospheres and 100 nm of carboxylate polystyrene nanospheres were obtained from Microspheres-Nanospheres Co., USA. Firstly, 100 μL of the diluted nanospheres were centrifuged and resuspended in 100 μL of the 70 % ethanol (v/v). Finally, 2 μL of this solution was introduced into the deep channel-A by capillary pressure.
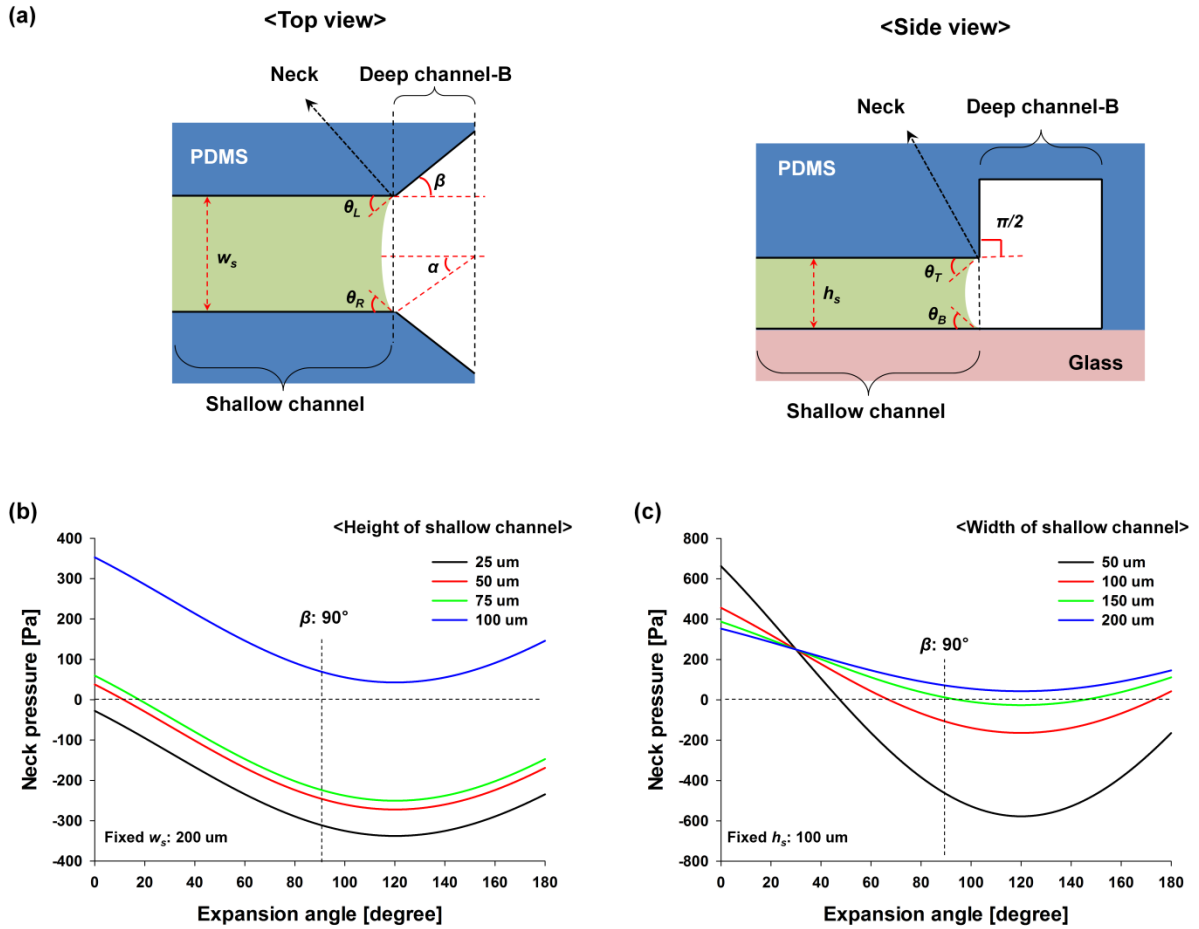
<Figure S2(c)>

Figure S3 (a) Schematic of the capillary flow of diluted nanoparticles at the neck of the shallow channel. (b) Theoretical neck pressure, P_n, by varying the expansion angle, β, and height of the shallow channel (c) P_n with respect to β and width of the shallow channel.

The diluted nanoparticles at the intersection between shallow and deep channel experience a sudden pressure drop (ΔP_{12}), which tries to drag the solution in the deep channel into the shallow channel ($F_{shallow}$).[1] When this flow of solution in shallow channel is located at the neck (interface between shallow channel and deep channel-B, Figure S3(a)), the capillary pressure at the neck (P_n) is induced and it can be expressed as below:[2]

$$P_n = \sigma(\frac{\sin\alpha}{\alpha}) \times (\frac{\cos(\theta_T + \pi/2) + \cos\theta_B}{h_s} + \frac{\cos(\theta_L + \beta) + \cos(\theta_R + \beta)}{w_s}) \qquad (S1)$$

here, σ, h_s, and w_s is the surface tension, the height of shallow channel, and the width of shallow channel, respectively. θ is the contact angle and the subscripts T, B, L, and R indicate the top, bottom, left and right surface of the shallow channel, respectively. α is the curvature angle and β is the expansion angle in the width direction. In these equations, the solution may move forward toward the deep channel-B when the capillary pressure at the neck, P_n, is positive, and stop at the neck when P_n is negative. Figure S3(b) shows the change of P_n as varying the expansion angle and the height of the shallow channel. The width of the shallow channel was fixed with 200 μm, the value of the surface tension with 0.025 N/m was used for 70 % of the ethanol,[3] and the contact angles were measured from the PDMS substrate (for θ_T, θ_L, and θ_R, ~60°) and glass substrate (for θ_B, ~45°). The negative P_n (stop pressure at the neck) are maximized at β around the 120° at 25, 50, and 75 μm of the h_s. If h_s is equal to the height of the deep channel (at 100 μm), the effect of the expansion angle at the top surface of the neck is neglected (*i.e.*, $\cos(\theta_T + \pi/2) \rightarrow \cos\theta_T$ in Equation S1) and P_n is positive for all β. However, this positive P_n can be adjusted to negative P_n by changing the width of the shallow channel, w_s, as shown in Figure S3(c). When w_s is lower than 150 μm, the positive P_n changes into negative around the β is 90° and the absolute value of negative P_n is maximized around the 120°. In this paper, 25 and 50 μm of the h_s, 200 um of the w_s, and 90° of the β is used to demonstrate the proposed RED systems, so that the capillary stop pressure at the neck is induced and the solution could not move forward toward the deep channel-B.

<Figure S2(d)>

After the solution stop at the neck, the evaporation of the solvent (70 % of the ethanol) is induced through the deep channel-B. Then the solvent with the convective transport of nanoparticles is introduced from the deep channel-A toward the neck to compensate of the solvent loss by evaporation. This influx of the nanoparticles promotes the growth of the ordered lattice (FCC structure) from neck to the deep channel-A in unidirectional. However, the careful selection of the size of the nanoparticles and the control of the Debye length, λ_D (it can be controlled by change of the material or ionic strength, and pH) are required because if the nanoparticles have strong repulsive interactions, the assembly to non-FCC structure can happen.[4] When the effective diameter (d_{eff}) of the spheres containing Debye

length is close to or larger than the center-to-center distance (d_c) between two spheres ($d_{eff} = d + 2\lambda_D > d_c$, wherein d is the diameter of the colloidal spheres), the colloidal spheres act like "hard spheres" and they will not influence each other until they are in physical contact.[4, 5] In this case, the FCC crystal structure is formed, and no heat or energy change is involved upon crystallization.
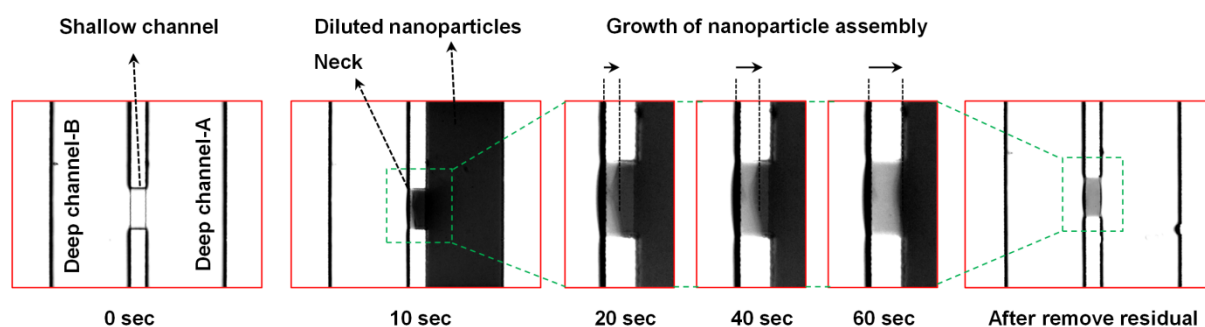
<Figure S2(e) and (f)>

Figure S4 Time sequence microscopic images of the *in situ* formation of nanochannel networks membrane using nanoparticles. Here, h_s and w_s was 50 μm and 200 μm, respectively, and the diameter with 300 nm of the silica nanospheres was used.

(e) When the growth of the nanoparticle assembly reaches the interface between the shallow channel and deep channel-A, the residual solution in deep channel-A is gently removed. Here, the growth of the nanoparticle assembly is easily observed by monitoring the change of the contrast of the light in the shallow channel through the inverted microscope (IX7, Olympus Co., Tokyo, Japan) as shown in Figure S4. (f) Finally, self-assembled nanoparticles are dried out in room temperature for one day.

S.3 Electrode calibration

Under asymmetric concentration of KCl solution, there exist additional electrode potential drop between two Ag/AgCl electrodes and it can be theoretically expressed by Nernst relation as follows:[6-8]

$$E_{redox} = \frac{R_g T}{zF} \ln \frac{\gamma_{c_H} c_H}{\gamma_{c_L} c_L} \tag{S2}$$

here, R_g is the universal gas, T is the absolute temperature, z is the valence of the ions, F is the Faraday constant, γ is the mean activity coefficient and c is the concentration at the membrane-solution interface, and the subscripts H and L indicate the high and low concentrated solution, respectively. We measured the electrode potential drop with the KCl solutions of varied concentration and compared with the theoretical E_{redox} for electrode calibration.

The experimental procedure of the electrode calibration was performed using the same size and shape of the main channels but without the shallow channel. Instead of the shallow channel, we connected the parallel main channel with the resistant of 1 GΩ, which is higher than the resistance of the electrodes and the KCl solution.[9] Then we introduced the KCl solution at 0.1 mM into the one side of the channel and obtained the *I-V* curve by changing the KCl solution of varied concentration of 1, 5, 10, 50, and 100 mM at the other side of channel, sequentially. Table S1 shows the comparison between the theoretical and experimental of electrode potential drops.

Table S1 Comparison between the theoretical and experimental of electrode potential drop

	0.1|1 mM	0.1|5 mM	0.1|10 mM	0.1|50 mM	0.1|100 mM
Theoretical	53.13 mV	98.76 mV	116.26 mV	156.90 mV	174.40 mV
Experimental	49.99 mV	82.17 mV	96.04 mV	128.25 mV	142.12 mV

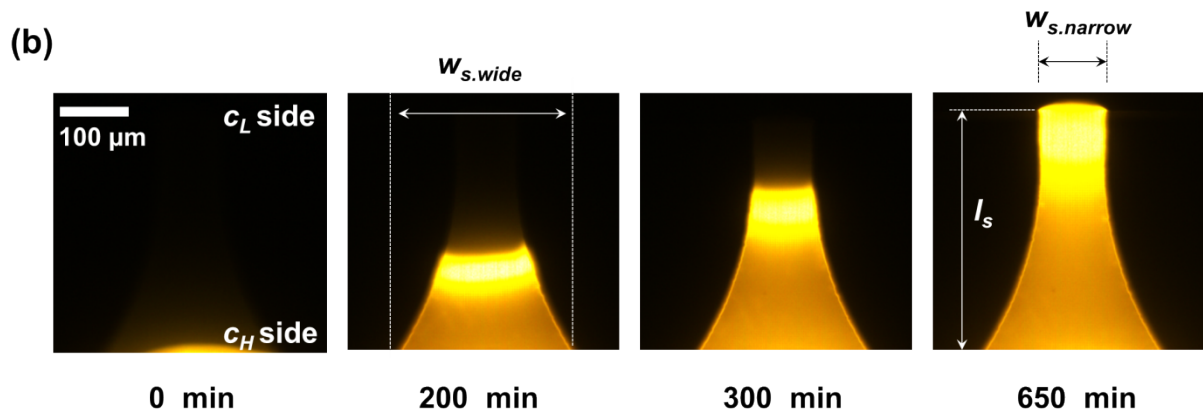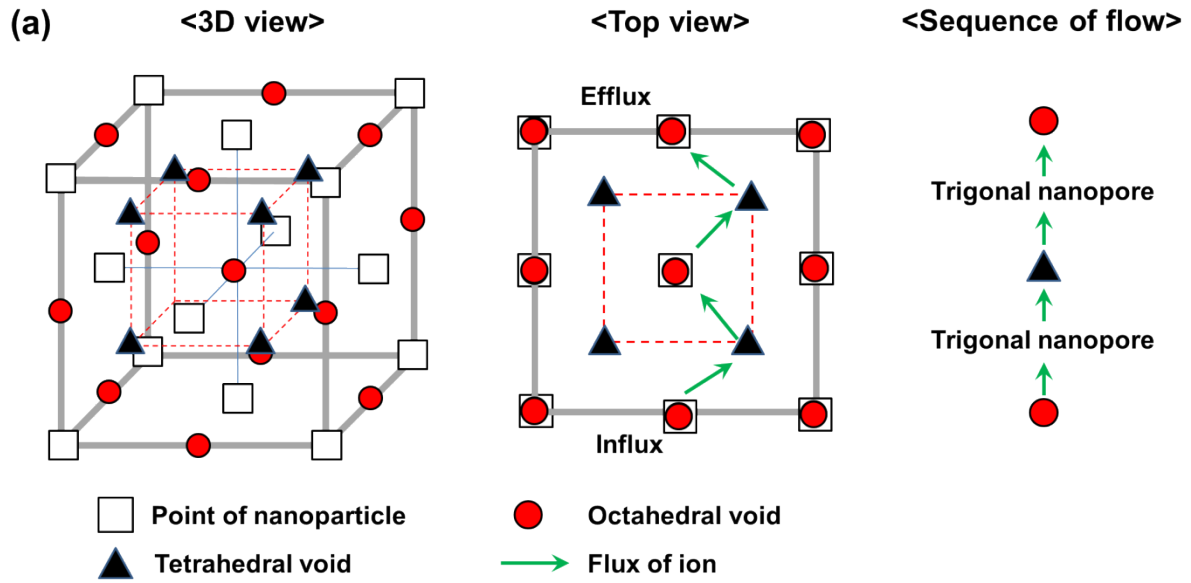## S.4 Evaluation of empirical constant, κ

(a)

(b)

Figure S5 (a) Scheme of the ion transport through the unit cell of the FCC structure. (b) Sequence image of the fluorescent dye transport through the proposed membrane.

The pure steric exclusion and hydrodynamic drag will lead the hindered diffusivity and Renkin`s equation provides a fraction (α_0) which is related between the nanopore diffusivity (D_{pore}) and the bulk diffusivity (D_{bulk}) when the ion transport through the single nanopore as below:[10]

$$\alpha_0 = \frac{D_{pore}}{D_{bulk}} = \left(1 - \frac{a}{r}\right)^2 \left[1 - 2.10\left(\frac{a}{r}\right) + 2.09\left(\frac{a}{r}\right)^3 - 0.95\left(\frac{a}{r}\right)^5\right] \quad (S3)$$

here, a and r is maximum steric radius of the counter-ion and the nanopore, respectively. We roughly assumed that each counter-ion is diffused in one-dimension, along the l_s with shortest path toward the lower concentration (<100> direction under the {100} plane of the FCC structure). Moreover, the diffusivity will decrease as multiplying by α_0 whenever the ion travels through the each nanopore. Therefore, the total fraction, α_{total} can be expressed as follows:

$$\alpha_{total} = \alpha_0^{\,\tau \cdot n \cdot \kappa} \qquad\qquad (S4)$$

where τ is the number of nanopores, n is the number of unit cells along the length of the shallow channel ($n = l_s (d\sqrt{2})^{-1}$, wherein d is the diameter of the nanoparticle), and κ is the empirical constant which are relevant to the enhancement of the diffusivity in nanopores due to the electrostatic attraction by the counter-charge on the surface of nanoparticles. Unlike the conventional organic membrane, we can easily infer the number of nanopores because the proposed membrane has highly ordered and close-packed FCC structure. As shown in Figure S5(a), there are four tetrahedral voids and thirteen octahedral voids (one in the center of the cell and twelve on the edge of the cell) in the unit cell of the close-packed FCC structure, and each voids are interconnected by trigonal nanopores. Therefore, when the ion transport across the membrane in shortest path toward the low concentration channel, it will experience four trigonal nanopores ($\tau = 4$) in the unit cell. κ is evaluated by performing the experiment for the ion transport through the proposed membrane using the positively charged fluorescent dye, rhodamine 6G (R6G) which represent the potassium ion as below:

As depicted in Figure S5(b), l_s, h_s, $w_{s.narrow}$, and $w_{s.wide}$ is 400 μm, 50 μm, 100 μm, and 290 μm, respectively. In addition, the diameter of R6G ($2r$), the diamter of silica nanoparticle (d), and nanopore diameter ($2a$) is 1.5 nm,[11] 300 nm, and 45 nm, respectively, and the bulk diffusivity of the R6G ($D_{R6G.bulk}$) in water, 25 °C, is 2.9×10^2 μm^2·sec^{-1}.[8] According to these parameters, the calculated βn and α_0 is 3768 and 0.86910563, respectively. We introduced the R6G at one side of the deep channel (c_H) and subsequently, we measured the time, t, for reaching the R6G to the opposite side of the deep channel (c_L) through the membrane by using the fluorescent microscope. Figure S5(b) shows the time

sequence fluorescent images and we obtained the *t* with 650 min. In these results and conditions, we obtained the diffusivity of the R6G in membrane ($D_{R6G.membrane}$) with value of ~ 2 $\mu m^2 \cdot sec^{-1}$ and finally, evaluated κ with the value of 0.009414666 by using Equation (S4), *i. e.*,

$$\alpha_{total} = D_{R6G.membrane} / D_{R6G.bulk} = 0.006896552 = 0.86910563^{3768\kappa}.$$

Reference

1. S. Chung, H. Yun and R. D. Kamm, *Small*, 2009, **5**, 609-613.

2. K. H. Chung, J. W. Hong, D.-S. Lee and H. C. Yoon, *Analytica Chimica Acta*, 2007, **585**, 1-10.

3. G. Vazquez, E. Alvarez and J. M. Navaza, *J Chem Eng Data*, 1995, **40**, 611-614.

4. Y. N. Xia, B. Gates, Y. D. Yin and Y. Lu, *Adv Mater*, 2000, **12**, 693-713.

5. T. Okubo, *Langmuir*, 1994, **10**, 1695-1702.

6. D.-K. Kim, C. Duan, Y.-F. Chen and A. Majumdar, *Microfluidics and Nanofluidics*, 2010, **9**, 1215-1224.

7. P. Läuger, *Angewandte Chemie International Edition in English*, 1969, **8**, 42-54.

8. A. J. Bard and L. R. Faulkner, *Electrochemical methods : fundamentals and applications / Allen J. Bard, Larry R. Faulkner*, Wiley, New York, 1980.

9. W. Guo, L. Cao, J. Xia, F.-Q. Nie, W. Ma, J. Xue, Y. Song, D. Zhu, Y. Wang and L. Jiang, *Advanced Functional Materials*, 2010, **20**, 1339-1344.

10. E. M. Renkin, *The Journal of General Physiology*, 1954, **38**, 225-243.

11. Y. Y. Kievsky, B. Carey, S. Naik, N. Mangan, D. ben-Avraham and I. Sokolov, *The Journal of Chemical Physics*, 2008, **128**, 151102.